11

# High-harmonic generation by interaction of frequency-spaced laser pulses with a graphene monolayer

© A.D. Panferov, A.A. Ulyanova

Saratov National Research State University,
Saratov, Russia

e-mail: panferovad@sgu.ru

*Received September 05, 2024*
*Revised October 02, 2024*
*Accepted October 27, 2024*

The features of the high-harmonic generation under conditions of simultaneous action of two laser pulses with different frequencies on graphene are investigated. For this purpose, a model based on a non-perturbative quantum kinetic equation was used. The normal incidence of short linearly polarized pulses with photon energies of 0.25 eV and 1.0 eV on the sample surface is considered. The polarization planes are chosen orthogonal to clearly identify nonlinear interaction effects. It is shown that under such conditions, the spectrum of high-frequency harmonics should be enriched and the efficiency of conversion of the energy of radiation incident on the sample to the high-frequency region should increase.

**Keywords:** high-harmonic, graphene monolayer, nonlinear effects, quantum kinetic equation.

DOI: 10.61011/EOS.2024.10.60060.7048-24

## Introduction

High-harmonic generation is a nonlinear optical phenomenon that is used not only for laser radiation frequency conversion in itself, but also for examining the ultrafast dynamics of electrons in various media. It has been observed for the first time in atomic gases [1]. As the capabilities for generation of high-intensity laser pulses expanded, the study of nonlinear regimes of interaction of condensed media with light has also become feasible [2,3]. The specifics of its band structure make graphene a standout material among those considered as candidate media for high-harmonic generation. The effect in this material has been observed experimentally in both terahertz [4,5] and mid-infrared [6,7] ranges. Various methods and approaches are used to characterize the observed processes theoretically [8–10]. Their refinement and development provides an opportunity to gain an insight into the complex physics of interaction of the electron subsystem of a material with an external electric field within a wide range of parameters and to model such processes. Nonlinear effects of mutual influence of fields with different characteristics and manifestations of such influence in secondary radiation spectra are of current interest [11–14].

The production and evolution of electrons and holes in two-level models of condensed matter have much in common with the processes associated with the production of electron–positron pairs from physical vacuum of quantum electrodynamics in strong electric fields. A non-perturbative kinetic formalism was developed [15–17] in order to characterize such processes. It allows one [18], e.g., to tackle the issue of „vacuum“ harmonic generation by laser radiation of an extreme intensity, which is important for nonlinear quantum electrodynamics [19–21].

A formalism of the quantum kinetic equation in the massless fermion approximation was developed for graphene based on the noted similarity [22–24]. Its capabilities for reproducing the spectral characteristics of induced radiation under the influence of short high-frequency pulses were demonstrated in [24,25]. A generalization for a more rigorous model with an exact account of the interaction of nearest neighbors in a two-dimensional hexagonal lattice has already been implemented [26]. This lifts the restrictions on parameters of the considered processes: the strength of the influencing electric field and its frequency.

In the present study, the quantum kinetic equation is used to study the specifics of high-harmonic generation under separate and combined influence of infrared frequency-spaced laser pulses on a sample.

## 1. Theoretical model

In order to reproduce the dynamics of the electron subsystem of graphene under a time-dependent external perturbing influence, one needs to solve the non-stationary Schrödinger equation in one of its representations. The main simplifying assumption used below is that the medium under study is regarded as a two-level system with a certain given dependence of the energy of states on their position in reciprocal space $\varepsilon(\mathbf{p})$. The dispersion law itself is determined from the stationary Schrödinger equation after specifying the explicit form of the Hamiltonian. Another simplifying factor is the assumption of spatial homogeneity of the perturbing effect at the interatomic scale, which is valid under the stated conditions. Since the system is two-

dimensional, all vector quantities under consideration are specified by two components.

Limiting ourselves to these two simplifications and defining the Hamiltonian in general form as

$$H(\mathbf{p},t)=\begin{pmatrix}0 & B'(\mathbf{p},t)+iB''(\mathbf{p},t)\\ B'(\mathbf{p},t)-iB''(\mathbf{p},t) & 0\end{pmatrix} \tag{1}$$

and the sought-for wave function in terms of the amplitudes of two pseudospin states

$$\Phi(\mathbf{p},t)=\begin{bmatrix}a(\mathbf{p},t)\\ b^{\dagger}(-\mathbf{p},t),\end{bmatrix} \tag{2}$$

we may obtain [23], without additional simplifying assumptions, a system of equations for the distribution functions of quasiparticles (electrons in the conduction band and holes in the valence band). To do this, one performs a transition to the occupation number representation with the substitution of amplitudes $a^{\dagger}(\mathbf{p},t)$, $a(\mathbf{p},t)$, $b^{\dagger}(\mathbf{p},t)$ $b(\mathbf{p},t)$ with the operators of creation and annihilation of the corresponding quasiparticles, which satisfy the canonical anticommutation relations

$$\{a(\mathbf{p},t),a^{\dagger}(\mathbf{p}',t)\}_{+}=\{b(\mathbf{p},t),b^{\dagger}(\mathbf{p}',t)\}_{+}=(2\pi)^2\delta(\mathbf{p}-\mathbf{p}'). \tag{3}$$

In the presence of a perturbing effect introducing an explicit time dependence into (1), the Fock space on which these operators act is defined on time-dependent vacuum states.

We assume that it is always possible to determine time $t_{in}$ of the onset of perturbation. Prior to this moment, the system was in a stationary state with eigen spectrum $\varepsilon(\mathbf{p})$ and vacuum state $|in\rangle$ that are set by the material characteristics. The distribution functions of electrons and holes are defined and considered in this initial basis:

$$f^{e}(\mathbf{p},t)=\langle in|\,a^{\dagger}(\mathbf{p},t)a(\mathbf{p},t)\,|in\rangle,$$
$$f^{h}(\mathbf{p},t)=\langle in|\,b^{\dagger}(-\mathbf{p},t)b(-\mathbf{p},t)\,|in\rangle. \tag{4}$$

Introducing auxiliary functions

$$u(\mathbf{p},t)=\frac{i}{2}\{\langle in|\,a^{\dagger}(\mathbf{p},t)b^{\dagger}(-\mathbf{p},t)\,|in\rangle - \langle in|\,b(-\mathbf{p},t)a(\mathbf{p},t)\,|in\rangle\},$$
$$v(\mathbf{p},t)=\frac{1}{2}\{\langle in|\,a^{\dagger}(\mathbf{p},t)b^{\dagger}(-\mathbf{p},t)\,|in\rangle + \langle in|\,b(-\mathbf{p},t)a(\mathbf{p},t)\,|in\rangle\}, \tag{5}$$

which characterize the polarization effects of interband transitions, and taking into account explicitly the condition of electrical neutrality of the medium $f^{e}(\mathbf{p},t)=f^{h}(\mathbf{p},t)=f(\mathbf{p},t)$, we obtain a closed system of equations for (4) and (5) [23]

$$\dot{f}(\mathbf{p},t)=\frac{\lambda(\mathbf{p},t)}{2}\,u(\mathbf{p},t),$$
$$\dot{u}(\mathbf{p},t)=\lambda(\mathbf{p},t)\big(1-2f(\mathbf{p},t)\big)-\frac{2\varepsilon(\mathbf{p},t)}{\hbar}\,v(\mathbf{p},t), \tag{6}$$
$$\dot{v}(\mathbf{p},t)=\frac{2\varepsilon(\mathbf{p},t)}{\hbar}\,u(\mathbf{p},t).$$

Here,

$$\varepsilon(\mathbf{p},t)=\sqrt{B'(\mathbf{p},t)^2+B''(\mathbf{p},t)^2}$$

is the current positive eigen value of time-dependent Hamiltonian (1) and

$$\lambda(\mathbf{p},t)=\frac{\dot{B}'(\mathbf{p},t)B''(\mathbf{p},t)-B'(\mathbf{p},t)\dot{B}''(\mathbf{p},t)}{\varepsilon^2(\mathbf{p},t)}. \tag{7}$$

Let the reason for the transition of a system with Hamiltonian $H(\mathbf{p})$ to a non-stationary regime be the influence of an external classical homogeneous electric field $\mathbf{E}(t)$. Introducing vector potential $\mathbf{A}(t)$ of this field by the $\mathbf{E}(t)=-\dot{\mathbf{A}}(t)$ condition in the Weyl gauge, which ensures that the scalar potential is equal to zero, we perform substitution

$$\mathbf{p}\to\mathbf{P}(t)=p-e\mathbf{A}(t), \tag{8}$$

where $e=-|e|$ is the electron charge. Substitution

$$H(\mathbf{p})\to H(\mathbf{p},t)=H\big(\mathbf{P}(t)\big) \tag{9}$$

will then yield an explicit form of this Hamiltonian under non-stationary conditions.

The explicit stationary form of the Hamiltonian is defined using the model of strong interaction of nearest neighbors. With substitution (9) taken into account, it takes the following form in the coordinate system with its origin at the center of the first Brillouin zone [27]:

$$B'\big(\mathbf{P}(t)\big)+iB''\big(\mathbf{P}(t)\big)=-\gamma\sum_{l}\exp\left(\frac{i}{\hbar}\,\mathbf{P}(t)\boldsymbol{\delta}_l\right), \tag{10}$$

where transition energy $\gamma\approx 2.7\,\text{eV}$ and vectors $\boldsymbol{\delta}_l$ specify the position of the three nearest neighbors for atoms of one of the sublattices. They following form may be chosen for them:

$$\boldsymbol{\delta}_1=\frac{a}{\sqrt{3}}(-1,0),\quad \boldsymbol{\delta}_2=\frac{a}{\sqrt{3}}\left(\frac{1}{2},\frac{\sqrt{3}}{2}\right),$$
$$\boldsymbol{\delta}_3=\frac{a}{\sqrt{3}}\left(\frac{1}{2},-\frac{\sqrt{3}}{2}\right). \tag{11}$$

Here, $a\approx 0.246\,\text{nm}$ is the lattice constant of graphene.

A coordinate system with its origin at the center of a primitive cell of the reciprocal lattice is more convenient for further analysis. The expressions for real and imaginary components of the Hamiltonian may then be reduced to the form

$$B'\big(\mathbf{P}(t)\big)=\gamma\left[\sin\left(\frac{P_1(t)a}{\sqrt{3}\hbar}+\frac{\pi}{6}\right)+\sin\left(\frac{P_1(t)a}{2\sqrt{3}\hbar}+\frac{P_2(t)a}{2\hbar}-\frac{\pi}{6}\right)+\sin\left(\frac{P_1(t)a}{2\sqrt{3}\hbar}-\frac{P_2(t)a}{2\hbar}-\frac{\pi}{6}\right)\right], \tag{12}$$

$$B''(\mathbf{P}(t)) = \gamma\left[\cos\left(\frac{P_1(t)a}{\sqrt{3}\hbar} + \frac{\pi}{6}\right) - \cos\left(\frac{P_1(t)a}{2\sqrt{3}\hbar} + \frac{P_2(t)a}{2\hbar} - \frac{\pi}{6}\right) - \cos\left(\frac{P_1(t)a}{2\sqrt{3}\hbar} - \frac{P_2(t)a}{2\hbar} - \frac{\pi}{6}\right)\right]. \quad (13)$$

In this case, the coefficients of system of equations (6) are determined explicitly:

$$\varepsilon(\mathbf{P}(t)) = \frac{2\hbar V_F}{\sqrt{3}a}\times \sqrt{3-4\cos\left(\frac{\sqrt{3}aP_1(t)}{2\hbar}\right)\cos\left(\frac{aP_2(t)}{2\hbar}\right)+2\cos\left(aP_2(t)/\hbar\right)}, \quad (14)$$

$$\lambda(\mathbf{P}(t)) = -\frac{4e\hbar V_F^2}{9a\varepsilon^2(\mathbf{P}(t))}\left[E_1(t)\sqrt{3}\left(\cos\left(\frac{\sqrt{3}aP_1(t)}{2\hbar}\right)\times\cos\left(\frac{aP_2(t)}{2\hbar}\right)+\cos\left(\frac{aP_2(t)}{\hbar}\right)\right) + E_2(t)3\sin\left(\frac{\sqrt{3}aP_1(t)}{2\hbar}\right)\sin\left(\frac{aP_2(t)}{2\hbar}\right)\right]. \quad (15)$$

Fermi velocity $V_F = \sqrt{3}\,a\gamma/2\hbar \cong 10^6$ m/s.

The characteristics of induced radiation are set by the surface density of currents generated in the sample by an external field. The components of surface current density for Hamiltonian (1) are expressed through the solutions of system (6) as [25]

$$j_k(t) = \int \frac{d^2p}{(2\pi\hbar)^2}\frac{1}{\varepsilon(\mathbf{P}(t))}\left\{\frac{\partial B'(\mathbf{P}(t))}{\partial P_k}\times\left[2B'(\mathbf{P}(t))f(\mathbf{p},t)+B''(\mathbf{P}(t))u(\mathbf{p},t)\right]+\frac{\partial B''(\mathbf{P}(t))}{\partial P_k}\times\left[2B''(\mathbf{P}(t))f(\mathbf{p},t)-B'(\mathbf{P}(t))u(\mathbf{p},t)\right]\right\},\ k=1,2. \quad (16)$$

Using expressions (12) and (13), we find

$$j_1(t) = j_1^{\text{cond}}(t) + j_1^{\text{pol}}(t) = e\frac{8V_F^2\hbar}{3a}\int\frac{d^2p}{(2\pi\hbar)^2}\sqrt{3}\times\left[1+2\cos\left(\frac{aP_1(t)}{\sqrt{3}\hbar}\right)\right]\sin\left(\frac{aP_1(t)}{2\sqrt{3}\hbar}\right)\cos\left(\frac{aP_2(t)}{2\hbar}\right)\times\frac{f(\mathbf{p},t)}{\varepsilon(\mathbf{P}(t))} - e\frac{4V_F^2\hbar}{3a}\int\frac{d^2p}{(2\pi\hbar)^2}\frac{1}{\sqrt{3}}\left[\cos\left(\frac{\sqrt{3}aP_1(t)}{2\hbar}\right)\times\cos\left(\frac{aP_2(t)}{2\hbar}\right)+\cos\left(\frac{aP_2(t)}{\hbar}\right)\right]\frac{u(\mathbf{p},t)}{\varepsilon(\mathbf{P}(t))}, \quad (17)$$

$$j_2(t) = j_2^{\text{cond}}(t) + j_2^{\text{pol}}(t) = e\frac{8V_F^2\hbar}{3a}\int\frac{d^2p}{(2\pi\hbar)^2}\times\left[\cos\left(\frac{\sqrt{3}aP_1(t)}{2\hbar}\right)\sin\left(\frac{aP_2(t)}{2\hbar}\right)-\sin\left(\frac{aP_2(t)}{\hbar}\right)\right]\times\frac{f(\mathbf{p},t)}{\varepsilon(\mathbf{P}(t))} - e\frac{4V_F^2\hbar}{3a}\int\frac{d^2p}{(2\pi\hbar)^2}\left[1+2\cos\left(\frac{aP_1(t)}{\sqrt{3}\hbar}\right)\right]\times\sin\left(\frac{aP_1(t)}{2\sqrt{3}\hbar}\right)\sin\left(\frac{aP_2(t)}{2\hbar}\right)\frac{u(\mathbf{p},t)}{\varepsilon(\mathbf{P}(t))}. \quad (18)$$

Each current component is represented as a sum of two terms. The first term is specified by distribution function $f(\mathbf{p},t)$ and represents the conduction current caused by intraband charge dynamics. The second term is characterized by function $u(\mathbf{p},t)$ and represents the polarization current sustained by the balance of creation and annihilation of pairs of electrons and holes. Integration must be performed over the entire Brillouin zone or its equivalent with the periodicity of the model's behavior in reciprocal space taken into account correctly.

System of equations (6) with explicitly defined coefficients (14) and (15) provides an opportunity to reproduce numerically the evolution of population of any state of the Brillouin zone under the influence of an electric field with an arbitrary time dependence. Observable currents (17) and (18) may be calculated by solving the kinetic equation in a sufficiently representative set of states. By virtue of the assumed spatial homogeneity of the model used, current density components $j_k(t)$ depend on time only.

The electric field produced at distance $z$ from an infinite plane with a uniform current density is given by [28]

$$E_k(t,z) = -\frac{\mu_0 c}{2}\,j_k\left(t-\frac{z}{c}\right), \quad (19)$$

where $\mu_0$ is the permeability of vacuum and $c$ is the speed of light. In a real-word environment, the dimensions of the region in which the influencing field remains uniform are limited, and expression (19) is applicable only in the near-field zone. However, the spectral composition of induced radiation is preserved in the process of propagation in free space.

High-harmonic generation is achieved in experiments with the use of short laser pulses with high energy density. Upon completion of such a pulse, the quantum system returns to a stationary state, although with a different population of bands. In the simplest case, the initial state may be a quasiparticle vacuum $f(\mathbf{p},t_{in}) = u(\mathbf{p},t_{in}) = v(\mathbf{p},t_{in}) = 0$ or an equilibrium thermodynamic distribution $f(\mathbf{p},t_{in}) \neq 0$ with uncorrelated (decoherent) states $u(\mathbf{p},t_{in}) = v(\mathbf{p},t_{in}) = 0$.

The solutions of system (6) reflect the dissipativeless quantum evolution of states. In real samples, relaxation processes may play a significant role even on a time scale of tens of femtoseconds [29,30]. These processes may be taken into account in the used approach in the relaxation

time approximation or by introducing two different time scales for the relaxation of population of excited states $\tau_r$ and decoherence $\tau_d$ [25,31]

$$\begin{aligned}\dot{f}(\mathbf{p},t) &= -\frac{\big(f(\mathbf{p},t)-f(\mathbf{p},t_{in})\big)}{\tau_r}+\frac{\lambda(\mathbf{p},t)}{2}u(\mathbf{p},t),\\ \dot{u}(\mathbf{p},t) &= -\frac{\big(u(\mathbf{p},t)-u(\mathbf{p},t_{in})\big)}{\tau_d}+\lambda(\mathbf{p},t)\big(1-2f(\mathbf{p},t)\big)\\ &\quad -\frac{2\varepsilon(\mathbf{p},t)}{\hbar}v(\mathbf{p},t),\\ \dot{v}(\mathbf{p},t) &= -\frac{\big(v(\mathbf{p},t)-v(\mathbf{p},t_{in})\big)}{\tau_d}+\frac{2\varepsilon(\mathbf{p},t)}{\hbar}u(\mathbf{p},t).\end{aligned} \tag{20}$$

## 2. Problem formulation

We used the following definition of field components to identify and study the effects of nonlinear interaction of two laser pulses with different frequencies:

$$E_1(t)=E_{10}e^{-t^2/(2\tau_1^2)}\left[\cos(2\pi\nu_1 t)-\frac{t}{2\pi\nu_1\tau_1^2}\sin(2\pi\nu_1 t)\right], \tag{21}$$

$$E_2(t)=E_{20}e^{-t^2/(2\tau_2^2)}\left[\cos(2\pi\nu_2 t)-\frac{t}{2\pi\nu_2\tau_2^2}\sin(2\pi\nu_2 t)\right]. \tag{22}$$

This provides an opportunity to specify them in a form close to that established in actual experiments and to set the components of vector potential for (9) by expressions

$$A_1(t)=-\frac{E_{10}}{2\pi\nu_1}e^{-t^2/(2\tau_1^2)}\sin(2\pi\nu_1 t), \tag{23}$$

$$A_2(t)=-\frac{E_{20}}{2\pi\nu_2}e^{-t^2/(2\tau_2^2)}\sin(2\pi\nu_2 t), \tag{24}$$

which ensure its equality to zero in both the initial and final states. The result is that the external electric field becomes a superposition of two pulses (each with its own frequency and duration) incident on the sample surface at a right angle and polarized linearly in orthogonal planes. The field components reach their maxima simultaneously at time point $t=0$. The values of $\nu_1=6.045\cdot10^{13}$ Hz and $\nu_2=2.418\cdot10^{14}$ Hz corresponding to photon energies of 0.25 and 1.0 eV were chosen. One needs to use an accurate model of interaction between nearest neighbors in order to obtain a correct description of processes proceeding under the influence of an external field with such frequencies. A four-fold frequency difference was chosen for the fact that, owing to isotropy of graphene, only odd harmonics are observed in the induced emission spectrum for single-frequency pulses, and the specified frequency spread provides an opportunity to separate the contributions of two pulses. The orthogonality of polarization directions serves the same purpose. The pulse durations were specified by $\tau_1=3.16\cdot10^{-14}$ s and $\tau_2=1.58\cdot10^{-14}$ s (a shorter high-frequency pulse is superimposed onto a low-frequency pulse). The amplitude values of field strength $E_{10}$ and $E_{20}$ used in modeling are given in the table. These values are set by conditions $eV_{\mathrm{F}}E_{k0}/2\pi\nu=0.05$ and $eV_{\mathrm{F}}E_{k0}/2\pi\nu=0.5$ eV, which are estimates of the maximum change in energy of states in the vicinity of Dirac points in an external field due to substitution (9). The influence of both individual pulses with the given parameters and their combinations was considered. It was assumed that the $f(\mathbf{p},t_{in})$ initial state is an equilibrium thermodynamic distribution corresponding to 20°C. Dissipative processes were taken into account by introducing relaxation time $\tau_r\approx100$ fs of non-equilibrium state population and decoherence time $\tau_d\approx10$ fs.

## 3. Results and discussion

Modeling was performed on 3-dimensional adaptive grids with a variable step in reciprocal space and a constant time step. Grids covering the reciprocal space were generated individually for each set of perturbing effect parameters in accordance with the procedure outlined in [32]. To ensure correct reproduction of integrals (17) and (18), the values of functions $f(\mathbf{p},t)$ and $u(\mathbf{p},t)$ were calculated for $\approx6\cdot10^4$–$4\cdot10^5$ states and $2.4\cdot10^3$ time steps.

At the first stage, the response of the model to independent action of individual pulses with frequencies $\nu_1$ and $\nu_2$ was calculated for two indicated values of each of the amplitudes $E_{10}$ and $E_{20}$. The resulting time dependence of the current density under the influence of only the first external field component (21) is shown in Fig. 1, *a*. The result corresponding only the second component (22) is presented in Fig. 1, *b*. The values of $E_{10}$ and $E_{20}$ differ; they are indicated in the figures and listed in the table. The pulse with higher frequency $\nu_2$ is two times shorter. A linear scale is used, but the current density values are scaled by a factor of 10 at the lower field strength for clarity. This corresponds to the ratio of electric field strength values and provides a clear illustration of nonlinearity of the dependence of the surface current density on this parameter. In both cases, the current components perpendicular to the influencing field are zero (within the calculation errors of the numerical procedures used).

To estimate the spectral composition of induced radiation, discrete series of $j_1$ and $j_2$ values were analyzed directly with account for (19). The frequency dependence of the squared Fourier transform modulus of current density component $k$ (power spectrum, which is hereinafter denoted as $S_k(\nu)$) was calculated. Since the simulated process was of a finite duration, the periodogram method with the Hann window function and averaging of the results over a sequence of overlapping samples (Welch's method) implemented in the Wolfram Mathematica package was used. The obtained power spectrum values were converted to a logarithmic scale via the $S_k(\nu)\to10\mathrm{Lg}\big(S_k(\nu)\big)$ transformation (with the $S_k(\nu)$ designation preserved) and expressed in arbitrary

Amplitude values of the electric field strength components, the corresponding peak energy flux densities, and estimates of the energy spectrum perturbation

| $E_{10}$, peak energy flux density at frequency $\nu_1$, variation of energy of states $eV_F E_{10}/2\pi\nu_1$ | $E_{20}$, peak energy flux density at frequency $\nu_2$, variation of energy of states $eV_F E_{20}/2\pi\nu_2$ |
|---|---|
| $1.899 \cdot 10^5$ V/cm, $4.78 \cdot 10^7$ W/cm$^2$, 0.05 eV | $7.59 \cdot 10^5$ V/cm, $7.65 \cdot 10^8$ W/cm$^2$, 0.05 eV |
| $1.899 \cdot 10^6$ V/cm, $4.78 \cdot 10^9$ W/cm$^2$, 0.5 eV | $7.59 \cdot 10^6$ V/cm, $7.65 \cdot 10^{10}$ W/cm$^2$, 0.5 eV |

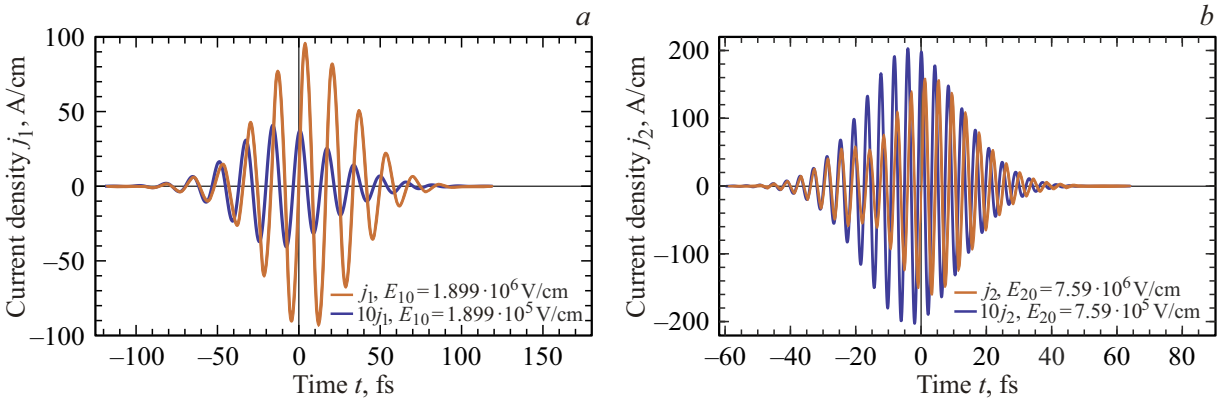


**Figure 1.** Time dependence of the first component of current density $j_1$ for external field pulses of the form (21) and $E_2(t) = 0$ ($a$). Time dependence of the second component of current density $j_2$ for external field pulses of the form (22) and $E_1(t) = 0$ ($b$).

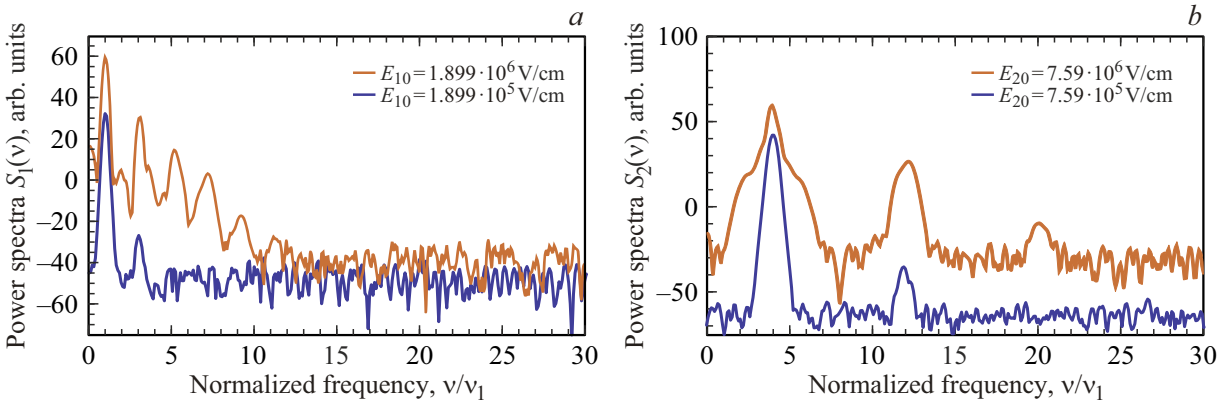


**Figure 2.** Power spectrum of surface currents in the case of independent action of pulses with frequencies ($a$) $\nu_1$ (external field is directed along the first coordinate axis) and ($b$) $\nu_2$ (external field is directed along the second coordinate axis).

units. Figure 2 presents the results for pulses with frequencies $\nu_1$ and $\nu_2$ acting independently on the sample. The response of the electron subsystem of the material at the carrier frequency ($\nu_1$ in Fig. 2, $a$ and $\nu_2(4\nu_1)$ in Fig. 2, $b$) is manifested clearly at all parameter combinations. At minimum external electric field strengths, third harmonics at frequencies $3\nu_1$ and $3\nu_2\,(12\nu_1)$, respectively, may be distinguished. When the electric field strength increases by an order of magnitude, a series of odd harmonics emerge: $3\nu_1$, $5\nu_1$, $7\nu_1$, $9\nu_1$, and $11\nu_1$ in Fig. 2, $a$ and $3\nu_2\,(12\nu_1)$ and $5\nu_2\,(20\nu_1)$ in Fig. 2, $b$. This agrees with the published estimates and results [6–10].

The effect of mutual influence of two pulses (Fig. 3) is manifested already at the minimum examined electric field strength. In the spectrum of the first current component $j_1$, no noticeable changes are found in the vicinity of frequencies $\nu_1$, $3\nu_1$, and $5\nu_1$; in the region of the fifth harmonic, the values remain at the background level. However, as one moves further to frequencies that may be associated with the seventh ($7\nu_1$) and ninth ($9\nu_1$) harmonics or defined as $2\nu_2 \pm \nu_1$, distinct bursts in the power spectrum with its values increasing by two orders of magnitude emerge (Fig. 3, $a$). Significant changes are also observed in the spectrum of the second current component $j_2$. The shape of response at the carrier frequency is preserved, but this line

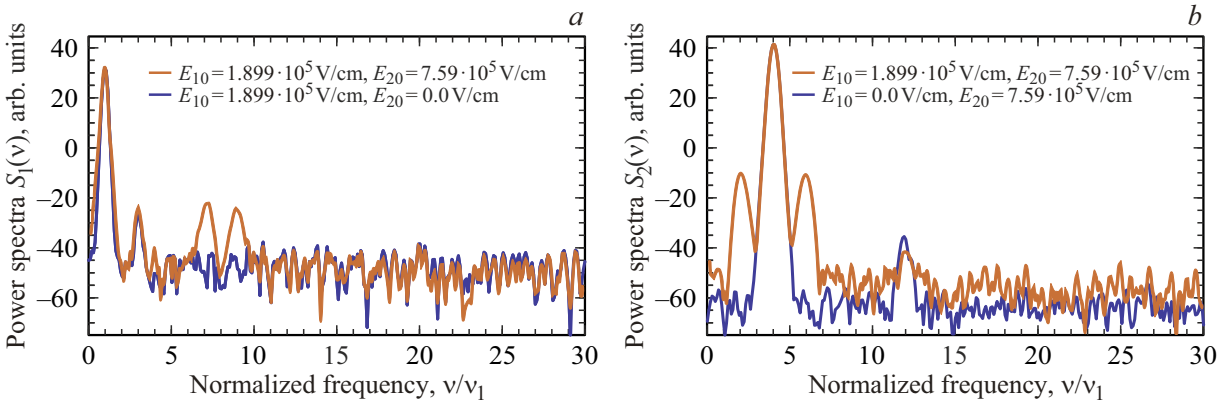


**Figure 3.** Comparison of $j_1$ power spectra for pulses with frequency $\nu_1$ and electric field amplitude $E_{01} = 1.899 \cdot 10^5$ V/cm calculated without and with a second pulse with frequency $\nu_2$ and $E_{02} = 7.59 \cdot 10^5$ V/cm ($a$). Comparison of $j_2$ power spectra for pulses with frequency $\nu_2$ and electric field amplitude $E_{02} = 7.59 \cdot 10^5$ V/cm calculated without and with a second pulse with frequency $\nu_1$ and $E_{01} = 1.899 \cdot 10^5$ V/cm ($b$).

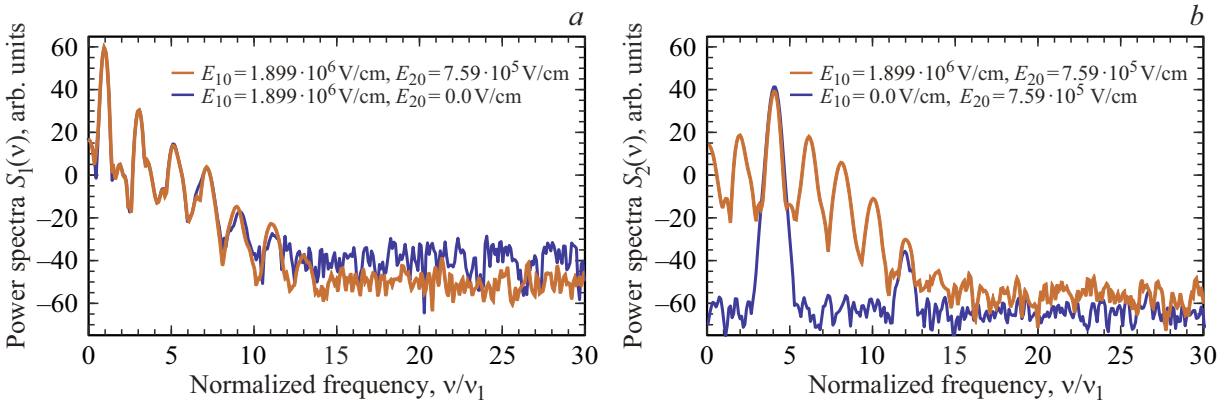


**Figure 4.** Comparison of $j_1$ power spectra for pulses with frequency $\nu_1$ and electric field amplitude $E_{01} = 1.899 \cdot 10^6$ V/cm calculated without and with a second pulse with frequency $\nu_2$ and $E_{02} = 7.59 \cdot 10^5$ V/cm ($a$). Comparison of $j_2$ power spectra for pulses with frequency $\nu_2$ and electric field amplitude $E_{02} = 7.59 \cdot 10^5$ V/cm calculated without and with a second pulse with frequency $\nu_1$ and $E_{01} = 1.899 \cdot 10^6$ V/cm ($b$).

acquires two symmetrical satellites at frequencies $\nu_2 \pm 2\nu_1$. The corresponding peaks are as much as five orders of magnitude above the initial individual pulse level (Fig. 3, $b$). One may also note the emergence of the zeroth harmonic.

Figure 4 presents the results obtained with the field strength of a low-frequency pulse increased by an order of magnitude. With the low-frequency pulse being dominant, the $j_1$ spectrum reveals no clear response to the presence or lack of an orthogonal high-frequency component (Fig. 4, $a$), featuring a well-pronounced series of odd harmonics. At the same time, the $j_2$ spectrum is transformed into a series of lines with a constant spacing of $2\nu_1$, which includes the zeroth harmonic. The values for the closest carrier satellites, $\nu_2 \pm 2\nu_1$, increase by as much as eight orders of magnitude (Fig. 4, $b$).

Figure 5 shows the results obtained in the opposite case (with the high-frequency component being dominant). The most profound changes are seen in the $j_1$ spectrum (Fig. 5, $a$). They may be interpreted as the emergence of additional lines with frequencies $2\nu_2 \pm \nu_1$ and $4\nu_2 \pm \nu_1$ with the observed values increasing by up to seven and five orders of magnitude, respectively. The formation of satellites with $\nu_1 \pm 0.5\nu_1$ in the immediate vicinity of carrier $\nu_1$ may also be identified. As for the $j_2$ spectrum, it does not reveal a clear response to the presence or lack of an orthogonal low-frequency component (Fig. 5, $b$).

The last pair of figures (Figs. 6, $a$ and $b$) present the results obtained in the case of interaction of pulses with maximum parameters. In this case, the spectra of both current components undergo significant changes attributable to mutual influences and become saturated with high-frequency harmonics through to $20-25\nu_1$.

The above results may be regarded as mutual stimulation of the process of high-harmonic generation under the combined influence of pulses with different frequencies. This is attributable both to an increase in the non-equilibrium population of states and to coherent coupling between transitions induced by the fields with different

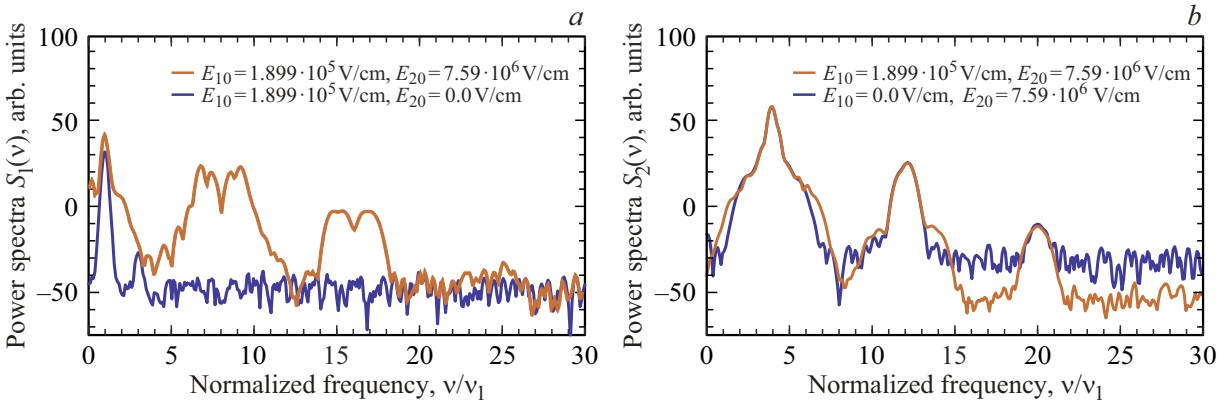


**Figure 5.** Comparison of $j_1$ power spectra for pulses with frequency $\nu_1$ and electric field amplitude $E_{01} = 1.899 \cdot 10^5$ V/cm calculated without and with a second pulse with frequency $\nu_2$ and $E_{02} = 7.59 \cdot 10^6$ V/cm $(a)$. Comparison of $j_2$ power spectra for pulses with frequency $\nu_2$ and electric field amplitude $E_{02} = 7.59 \cdot 10^6$ V/cm calculated without and with a second pulse with frequency $\nu_1$ and $E_{01} = 1.899 \cdot 10^5$ V/cm $(b)$.

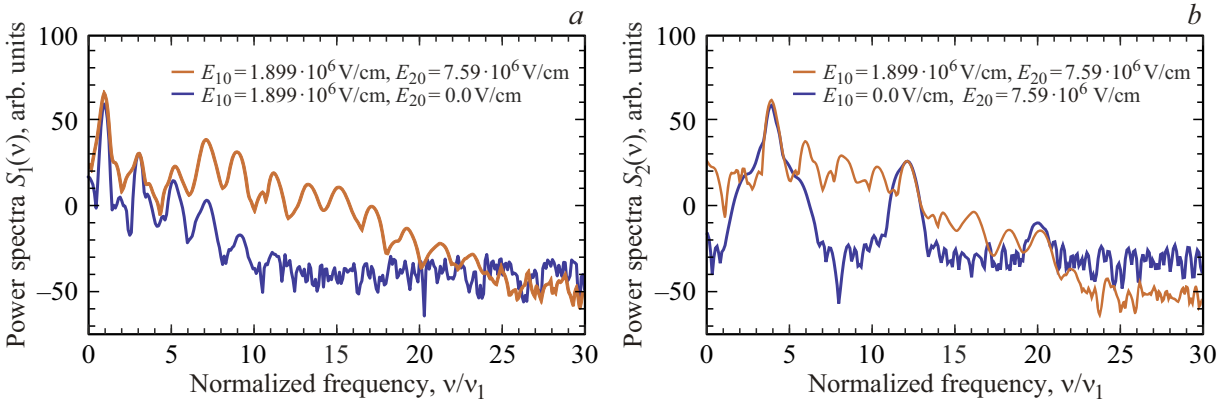


**Figure 6.** Comparison of $j_1$ power spectra for pulses with frequency $\nu_1$ and electric field amplitude $E_{01} = 1.899 \cdot 10^6$ V/cm calculated without and with a second pulse with frequency $\nu_2$ and $E_{02} = 7.59 \cdot 10^6$ V/cm $(a)$. Comparison of $j_2$ power spectra for pulses with frequency $\nu_2$ and electric field amplitude $E_{02} = 7.59 \cdot 10^6$ V/cm calculated without and with a second pulse with frequency $\nu_1$ and $E_{01} = 1.899 \cdot 10^6$ V/cm $(b)$.

frequencies [14]. The relative proximity of frequencies of the two pulses in the case under consideration enables the observation of harmonics with frequencies $\nu_2 \pm 2\nu_1$ and other similar combinations. It should be noted that numerical experiments with other frequency ratios are needed for an unambiguous determination of the frequencies of new harmonics through $\nu_1$ and $\nu_2$. The emergence of new harmonics outside the odd series may also be interpreted as a sign of violation of isotropy of the material properties.

## 4. Conclusion

The results of simulation of the response of the electron subsystem of graphene to the influence of an external electric field performed with the use of the quantum kinetic equation formalism based on a rigorous model of strong interaction of nearest neighbors were presented. It was demonstrated that the surface current reproduced using this approach for linearly polarized pulses with the considered parameters is parallel to the polarization plane and may feature a number of odd high harmonics alongside with the dominant contribution at the carrier frequency. This determines the characteristics of secondary induced radiation. The result is in close agreement with theory and experiment.

A significant mutual influence, which is manifested as an increase in the contribution of high-frequency harmonics to the surface current, was observed in modeling of the simultaneous action of two pulses with different parameters polarized linearly in orthogonal planes. A number of new harmonics emerged in the surface current spectrum both above the carrier frequency outside the odd series and in the low-frequency region. The obtained results are indicative of an increased efficiency of nonlinear conversion of laser pulse energy into the high-frequency region under the examined conditions.

### Funding

This study was supported by the Russian Science Foundation, grant №23-21-00047, https://rscf.ru/project/23-21-00047/.

### Conflict of interest

The authors declare that they have no conflict of interest.

## References

[1] M. Ferray, A. L'Huillier, X.F. Li, L.A. Lompre, G. Mainfray, C. Manus. J. Phys. B: At. Mol. Opt. Phys., **21** (3), L31–L35 (1988). DOI: 10.1088/0953-4075/21/3/001
[2] Sh. Ghimire, A.D. DiChiara, E. Sistrunk, P. Agostini, L.F. DiMauro, D.A. Reis. Nature Physics, **7**, 138–141 (2011). DOI: 10.1038/NPHYS1847
[3] Sh. Ghimire, D.A. Reis. Nature Physics, **15**, 10–16 (2019). DOI: 10.1038/s41567-018-0315-5
[4] H.A. Hafez, S. Kovalev, J-Ch. Deinert, Z. Mics, B. Green, N. Awari, M. Chen, S. Germanskiy, U. Lehnert, J. Teichert, Z. Wang, K-J. Tielrooij, Z. Liu, Z. Chen, A. Narita, K. Müllen, M. Bonn, M. Gensch, D. Turchinovich. Nature, **561**, 507–511 (2018). DOI: 10.1038/s41586-018-0508-1
[5] S. Kovalev, H.A. Hafez, K-J. Tielrooij, J-Ch. Deinert, I. Ilyakov, N. Awari, D. Alkaraz, K. Soundarapandian, D. Saleta, S. Germanskiy, M. Chen, M. Bawatna, B. Green, F.H.L. Koppens, M. Mittendorf, M. Bonn, M. Gensch, D. Turchinovich. Sci. Adv., **7** (15), eabf9809 (2021). DOI: 10.1126/sciadv.abf9809
[6] N. Yoshikawa, T. Tamaya, K. Tanaka. Science, **356**, 736–738 (2017). DOI: 10.1126/science.aam8861
[7] S. Cha, M. Kim, Y. Kim, Sh. Choi, S. Kang, H. Kim, S. Yoon, G. Moon, T. Kim, Y.W. Lee, G.Y. Cho, M.J. Park, Ch.-J. Kim, B.J. Kim, J.D. Lee, M-H. Jo, J. Kim. Nature Commun., **13**, 6630 (2022). DOI: 10.1038/s41467-022-34337-y
[8] K.L. Ishikawa. Phy. Rev. B., **82**, 201402 (2010). DOI: 10.1103/PhysRevB.82.201402
[9] I. Al-Naib, J.E. Sipe, M.M. Digman. New J. Phys., **17**, 113018 (2015). DOI: 10.1088/1367-2630/17/11/113018
[10] M. Ornigotti, D.N. Carvalho, F. Biancalana. Riv. Nuovo Cim., **46**, 295–380 (2023). DOI: 10.1007/s40766-023-00043-8
[11] H.K. Avetissian, A.K. Avetissian, B.R. Avchyan, G.F. Mkrtchian. Phys. Rev. B, **100**, 035434 (2019). DOI: 10.1103/PhysRevB.100.035434
[12] M.S. Mrudul, Á. Jimenez-Galan, M. Ivanov, G. Dixit. Optica, **8** (3), 422–427 (2021). DOI: 10.1364/OPTICA.418152
[13] H.K. Avetissian, G.F. Mkrtchian, A. Knorr. Phys. Rev. B, **105**, 195405 (2022). DOI: 10.1103/PhysRevB.105.195405
[14] W. Mao, A. Rubio, Sh.A. Sato. Phys. Rev. B, **109**, 045421 (2024). DOI: 10.1103/PhysRevB.109.045421
[15] A.A. Grib, S.G. Mamaev, V.M. Mostepanenko. *Vakuumnye kvantovye effekty v sil'nykh polyakh* (Energoatomizdat, M., 1988) (in Russian).
[16] S.M. Schmidt, D. Blaschke, G. Röpke, S.A. Smolyansky, A.V. Prozorkevich, V.D. Toneev. Int. J. Mod. Phys. E, **7** (6), 709 (1998). DOI: 10.1142/S0218301398000403
[17] D.B. Blaschke, A.V. Prozorkevich, G. Röpke, C.D. Roberts, S.M. Schmidt, D.S. Shkirmanov, S.A. Smolyansky. Eur. Phys. J. D, **55**, 341 (2009). DOI: 10.1140/epjd/e2009-00156-y
[18] I.A. Aleksandrov, A.D. Panferov, S.A. Smolyansky. Phys. Rev. A, **103**, 053107 (2021). DOI: 10.1103/PhysRevA.103.053107
[19] P.V. Sasorov, F. Pegoraro, T.Zh. Esirkepov, S.V. Bulanov. New J. Phys., **23**, 105003 (2021). DOI: 10.1088/1367-2630/ac28cb
[20] A. Fedotov, A. Ilderton, F. Karbstein, B. King, D. Seipt, H. Taya, G. Torgrimsson. Phys. Reports, **1010**, 1 (2023). DOI: 10.1016/j.physrep.2023.01.003
[21] V.V. Dmitriev, S.A. Smolyansky, V.A. Tseryupa. Physics of Atomic Nuclei, **86**, 913 (2023). DOI: 10.1134/S1063778823050137
[22] A. Panferov, S. Smolyansky, D. Blaschke, N. Gevorgyan. EPJ Web Conf., **204**, 060089 (2019). DOI: 10.1051/epjconf/201920406008
[23] S.A. Smolyansky, A.D. Panferov, D.B. Blaschke, N.T. Gevorgyan. Particles, **2**, 208 (2019). DOI: 10.3390/particles2020015
[24] S.A. Smolyansky, D.B. Blaschke, V.V. Dmitriev, A.D. Panferov, N.T. Gevorgyan. Particles, **3**, 456 (2020). DOI: 10.3390/particles3020032
[25] A.D. Panferov, N.A. Novikov. Izv. Sarat. Univ. Nov. Ser. Ser.: Fiz., **23** (3), 254 (2023) (in Russian). DOI: 10.18500/1817-3020-2023-23-3-254-264
[26] A.D. Panferov, I.A. Shcherbakov. Izv. Sarat. Univ. Nov. Ser. Ser.: Fiz., **24** (3), 198 (2024) (in Russian). DOI: 10.18500/1817-3020-2023-24-3-198-208
[27] M.I. Katsnelson. *The Physics of Graphene*. 2nd edn. (Cambridge University Press, 2020).
[28] T.A. Abbott, D.J. Griffiths. Am. J. Phys., **53**, 1203–1211 (1985). DOI: 10.1119/1.14084
[29] Chr. Heide, T. Eckstein, T. Boolakee, C. Gerner, H.B. Weber, I. Franco, P. Hommelhoff. Nano Lett., **21**, 9403–9409 (2021). DOI: 10.1021/acs.nanolett.1c02538
[30] Y. Kim, M.J. Kim, S. Cha, Sh. Choi, Ch-J. Kim, B.J. Kim, M.-H. Jo, J. Kim, J.D. Lee. Nano Lett., **24**, 1277–1283 (2024). DOI: 10.1021/acs.nanolett.3c04278
[31] A.D. Panferov, N.A. Novikov. In *Vzaimodeistvie sverkhvysokochastotnogo, teragertsovogo i opticheskogo izlucheniya s poluprovodnikovymi mikro- i nanostrukturami, metamaterialami i bioob"ektami: Sbornik statei odinnadtsatoi Vserossiiskoi nauchnoi shkoly-seminara* (Sarat. Istochnik, Saratov, 2024), pp. 89–93 (in Russian).
[32] A.D. Panferov, N.V. Posnova, A.A. Ul'yanova. Program. Sist.: Teor. Prilozh., **14** (2), 27–47 (2023) (in Russian). DOI: 10.25209/2079-3316-2023-14-2-27-47

*Translated by D.Safin*